

An analysis of the longitudinal structure function at next-to-leading order approximation at small- x

G.R.Boroun*

Department of Physics, Razi University, Kermanshah 67149, Iran

Yanbing Cai†

*Guizhou Key Laboratory in Physics and Related Areas,
Guizhou University of Finance and Economics, Guiyang 550025, China*

(Dated: December 12, 2024)

The longitudinal structure function is considered at the next-to-leading order approximation using the expansion method, as defined by M.B.Gay Ducati and P.B.Goncalves [Phys.Lett.B **390**, 401 (1997)] and further developed by Jingxuan Chen et al., [Chin.Phys.C **48**, 063104 (2024)]. This method provides results for a wide range of x and Q^2 values. It is observed that the behavior of the longitudinal structure function depends on the fractional momentum carried by gluons at low x . The extracted longitudinal structure functions $F_L(x, Q^2)$ are in line with data from the H1 Collaboration [V. Andreev et al. (H1 Collaboration), Eur. Phys. J. C **74**, 2814 (2014)] and the CT18 parametrization method [T.-J. Hou et al., Phys. Rev. D **103**, 014013 (2021)].

Introduction

Quantum chromodynamics (QCD) is a theory describing the strong interaction, in which the fundamental degrees of freedom are quarks and gluons [1]. Determining the inner quark and gluon constituents of the proton is crucial for QCD applications, as it is a key ingredient in QCD factorization calculations. Unlike the naive quark parton model [2], which suggests that the proton is composed solely of quarks, QCD reveals a more intricate structure for the proton, including not only quarks but also anti-quarks and gluons. The probability distribution of these constituents within the nucleon is known as parton distribution functions (PDFs), defined as the probability density for finding a parton with a longitudinal momentum fraction x at resolution scale Q^2 . However, due to the non-perturbative nature of partons, PDFs can not be calculated using perturbative QCD. Fortunately, high-energy lepton-nucleon scattering offers a unique opportunity to determine and test the partonic structure of the proton [3]. Pioneering deep inelastic electron-proton scattering (DIS) experiments conducted at SLAC have confirmed the partonic substructure of the proton [4, 5]. Additionally, DIS measurements by the H1 and ZEUS Collaborations at HERA have been used to extract the proton's parton distributions based on the factorization theorem [6]. The future Electron-Ion Colliders (EIC) [7] and Electron-Ion Colliders in China (EicC) [8] are expected to generate more high-precision DIS data, significantly improving our understanding of proton structure.

In the DIS process, the reduced neutral current differential cross section can be expressed in terms of three proton structure functions F_2 , xF_3 , and F_L [3]. These structure functions are related to the proton's parton distributions. The electromagnetic structure function F_2 is associated with pure photon exchange and represents the dominant contribution to the cross section across most of the kinematic range. The structure function xF_3 captures the difference between electron-proton and positron-proton cross sections. Within the framework of the quark parton model, xF_3 is directly related to valence-quark distributions. Consequently, measuring xF_3 provides insights into the lower- x behavior of these valence-quark distributions. The longitudinal structure function F_L is proportional to the cross section for interactions involving a longitudinally polarized virtual photon interacting with a proton. Notably, at leading order in QCD, F_L vanishes; however, it may become non-zero when gluon contributions are taken into account [9]. In the small- x region, the contribution from gluons significantly surpasses that of quarks. This results in F_L being directly sensitive to the gluon density, thereby serving as a direct measure of the gluon distribution [10].

*Electronic address: boroun@razi.ac.ir

†yanbingcai@mail.gufe.edu.cn

The longitudinal structure function has been measured by the H1 and ZEUS collaborations [11–14] and has been updated in Ref. [15], enhancing experimental precision and extending coverage across a broader kinematic range. These measurements provide significant constraints on the gluon distribution within the proton, as the longitudinal structure function can be obtained from the gluon distribution [16]. In the literature, the longitudinal structure function has been analytically examined through the gluon distribution which has been expanded at $z = 0$ [17] and at $z = \alpha$ (where $0 \leq \alpha < 1$) [18]. In our previous paper, we derived an analytical gluon distribution at low x based on the DGLAP equation, utilizing approximated leading-order (LO) and next-to-leading-order (NLO) splitting functions [19]. The analytical distribution provides a good description of the differential structure function. In this paper, we extend this analytical distribution to explore the longitudinal structure function. We find that our analytical results are consistent with data from the H1 Collaboration and the CT18 parametrization method.

Method

Recently, authors in Ref.[19] presented an analytical solution for the derivative of the proton structure function with respect to $\ln Q^2$, denoted as $\frac{\partial F_2(x, Q^2)}{\partial \ln Q^2}$. This solution was derived using the gluon distribution at the leading-order (LO) and the next-to-leading order (NLO) approximations in the small- x limit. The analysis is based on the expansion method at the expansion point $z = \alpha$ as reported in Refs.[20–22]. In Ref.[19], the gluon distribution from DGLAP evolution equations [23–25] using the Mellin transform was obtained. By neglecting the quark distribution at small- x , the evolution of the gluon density at the NLO approximation is defined by the following form

$$\frac{\partial g(x, Q^2)}{\partial \ln Q^2} = \frac{\alpha_s(Q^2)}{2\pi} \int_x^1 \left[2N + \frac{\alpha_s(Q^2)}{2\pi} \left(\frac{4}{3} C_F T_f - \frac{46}{9} N T_f \right) \right] g\left(\frac{x}{z}, Q^2\right) \frac{dz}{z^2}, \quad (1)$$

where the splitting functions at the LO and NLO approximations, at small fraction momentum, can be approximated as

$$P_{gg}^{\text{LO+NLO}}|_{z \ll 1} \approx \frac{1}{z} \left[2N + \frac{\alpha_s(Q^2)}{2\pi} \left(\frac{4}{3} C_F T_f - \frac{46}{9} N T_f \right) \right]. \quad (2)$$

For the SU(N) gauge group, we have $C_A = N$, $C_F = \frac{N^2-1}{2N}$, $T_f = n_f T_R$ and $T_R = 1/2$ where C_F and C_A are the color Casimir operators.

The DGLAP evolution equation for the gluon distribution function can be rewritten into the Mellin transform using the fact that the Mellin transform of a convolution factors is simply the ordinary product of the Mellin transform of the factors by the following form

$$G_\omega(x, Q^2) = \exp\left(\frac{1}{\omega} \eta(Q_0^2, Q^2)\right) G_\omega(x, Q_0^2), \quad (3)$$

where

$$\eta(Q_0^2, Q^2) = \int_{Q_0^2}^{Q^2} \frac{dq^2}{q^2} \frac{\alpha_s(q^2)}{2\pi} \left[2N + \frac{\alpha_s(q^2)}{2\pi} \left(\frac{4}{3} C_F T_f - \frac{46}{9} N T_f \right) \right]. \quad (4)$$

The inverse Mellin transform of the coefficients is straightforward as

$$G(x, Q^2) = \int_{a-i\infty}^{a+i\infty} \frac{d\omega}{2\pi i} \exp(P(\omega)) G_\omega(x, Q_0^2), \quad (5)$$

where

$$P(\omega) = \omega \ln \frac{1}{x} + \frac{1}{\omega} \eta(Q_0^2, Q^2). \quad (6)$$

The analytical solution for the gluon distribution, after some rearranging, is obtained in Ref.[19] in the following form

$$G(x, Q^2) = K(Q^2) I_0(2(\rho \ln(1/x))^d), \quad (7)$$

where

$$K(Q^2) = a[\exp(\xi - \xi_0) + b] \exp[c(\xi - \xi_0)^{1/2}], \quad (8)$$

with $\xi = \ln \ln(Q^2/\Lambda^2)$ and $\xi_0 = \ln \ln(Q_0^2/\Lambda^2)$ where Λ is the QCD cut-off parameter. The function ρ at the LO approximation is defined as

$$\rho(Q^2) = \frac{4N}{\beta_0} \ln \frac{t}{t_0}, \quad (9)$$

where $t = \ln \frac{Q^2}{\Lambda^2}$, $t_0 = \ln \frac{Q_0^2}{\Lambda^2}$ and $\beta_0 = \frac{1}{3}(33 - 2n_f)$. At the NLO approximation the function ρ is modified by the following form

$$\rho(Q^2) = \frac{4N}{\beta_0} \ln \frac{t}{t_0} R(t), \quad (10)$$

where

$$R(t) = \frac{\tilde{a}t^{\tilde{d}}}{\tilde{b} + \tilde{c}t^{\tilde{e}}}. \quad (11)$$

The coefficients at the LO and NLO approximations were determined to fit the CJ15LO [26] and CJ15NLO [27] data with $Q_0^2 = 1 \text{ GeV}^2$ and 2.5 GeV^2 respectively.

At small values of x , the longitudinal structure function is driven mainly by gluons as the Altarelli and Martinelli [16] equation for the gluonic longitudinal structure function $F_L^g(x, Q^2)$ is defined

$$F_L^g(x, Q^2) = \langle e^2 \rangle C_{L,g}(\alpha_s(Q^2), x) \otimes xg(x, Q^2) = \langle e^2 \rangle \int_x^1 \frac{dz}{z} C_{L,g}(\alpha_s(Q^2), z) G\left(\frac{x}{z}, Q^2\right), \quad (12)$$

where $\langle e^2 \rangle$ is the average charge for the active quark flavors, $\langle e^2 \rangle = n_f^{-1} \sum_{i=1}^{n_f} e_i^2$, and $C_{L,g}$ is the coefficient function that can be written by the perturbative expansion at the LO and NLO approximations as follows [28]

$$C_{L,g}(\alpha_s, x) = \frac{\alpha_s}{4\pi} c_{L,g}^{\text{LO}}(x) + \left(\frac{\alpha_s}{4\pi}\right)^2 c_{L,g}^{\text{NLO}}(x), \quad (13)$$

where $c_{L,g}^{\text{LO}}(z) = 8n_f z^2(1-z)$ and $c_{L,g}^{\text{NLO}}(z)|_{z \rightarrow 0} \approx -5.333n_f$.

Cooper-Sarkar et al in Ref.[17] have suggested that the longitudinal structure function by expansion of the gluon density around $z = 0$ has the following form

$$F_L(x, Q^2) \simeq \frac{\alpha_s(Q^2) \sum_f e_i^2}{3\pi} \frac{6}{5.9} G(2.5x, Q^2). \quad (14)$$

Authors in Ref.[18] extended Eq.(12) based on expanding the gluon distribution around $z = \alpha$ as the gluon distribution can be expanded using the expansion method at an arbitrary point $z = \alpha$ by the following form

$$G\left(\frac{x}{1-z}\right)|_{z=\alpha} = G\left(\frac{x}{1-\alpha}\right) + \frac{x}{1-\alpha}(z-\alpha) \frac{\partial G\left(\frac{x}{1-\alpha}\right)}{\partial x} + \mathcal{O}(z-\alpha)^2, \quad (15)$$

where the series is convergent for $|z - \alpha| < 1$ as

$$\frac{x}{1-z}|_{z=\alpha} = \frac{x}{1-\alpha} \sum_{k=1}^{\infty} \left[1 + \frac{(z-\alpha)^k}{(1-\alpha)^k}\right]. \quad (16)$$

The longitudinal structure function at the LO approximation is defined [18] by the following form

$$F_L(x, Q^2) \simeq \frac{\alpha_s(Q^2) \sum_f e_i^2}{3\pi} \frac{6}{5.9} G\left(\frac{x}{1-\alpha} \left(\frac{3}{2} - \alpha\right), Q^2\right), \quad (17)$$

where this result is similar to Eq.(14) when the expansion point $\alpha = 0.666$ is used. In the NLO approximation, the longitudinal structure function is given by

$$F_L(x, Q^2) \simeq F_L^{\text{LO}}(x, Q^2) (\text{i.e., Eq.(10)}) - 5.333 \sum_{i=1}^{n_f} e_i^2 \left(\frac{\alpha_s}{4\pi} \right)^2 \int_0^{1-x} \frac{dz}{1-z} G\left(\frac{x}{1-z}, Q^2\right). \quad (18)$$

The integral in Eq.(18) is modified by the following form

$$\int_0^{1-x} \frac{dz}{1-z} G\left(\frac{x}{1-z}, Q^2\right) = \frac{1}{x} \int_0^{1-x} d\tilde{z} \tilde{G}\left(\frac{x}{1-\tilde{z}}, Q^2\right), \quad (19)$$

where $\tilde{G}(x, Q^2) = xG(x, Q^2)$. In the limit $x \rightarrow 0$, the expansion of \tilde{G} around the point $z = \alpha$ gives [19]

$$\frac{1}{x} \int_0^{1-x} d\tilde{z} \tilde{G}\left(\frac{x}{1-\tilde{z}}, Q^2\right) = (1-x) \frac{\frac{3}{2} - 2\alpha}{(1-\alpha)^2} G\left(\frac{\frac{3}{2} - 2\alpha}{(1-\alpha)^2} x, Q^2\right). \quad (20)$$

Therefore, the gluonic longitudinal structure function in the NLO approximation is find

$$F_L(x, Q^2) \simeq \frac{\alpha_s(Q^2) \sum_f e_f^2}{3\pi} \frac{6}{5.9} G\left(\frac{x}{1-\alpha} \left(\frac{3}{2} - \alpha\right), Q^2\right) - 5.333 \sum_{i=1}^{n_f} e_i^2 \left(\frac{\alpha_s}{4\pi} \right)^2 (1-x) \frac{\frac{3}{2} - 2\alpha}{(1-\alpha)^2} G\left(\frac{\frac{3}{2} - 2\alpha}{(1-\alpha)^2} x, Q^2\right). \quad (21)$$

We observe that the longitudinal structure function is dependent on the gluon distribution at the expansion point $z = \alpha$. Indeed, the free parameter α relates the gluon density to the observable longitudinal structure function. Comparing with the high precision data for the longitudinal structure function at small x help to confirm the effectiveness of the approach and clarify what is the best value for the expansion point α in the next section.

Results and Discussion

The running coupling at the LO and NLO approximations are defined by the following forms

$$\begin{aligned} \alpha_s(Q^2) &= \frac{4\pi}{\beta_0 \ln(Q^2/\Lambda^2)} & (\text{LO}) \\ \alpha_s(Q^2) &= \frac{4\pi}{\beta_0 \ln(Q^2/\Lambda^2)} \left[1 - \frac{\beta_1 \ln \ln(Q^2/\Lambda^2)}{\beta_0^2 \ln(Q^2/\Lambda^2)} \right] & (\text{NLO}), \end{aligned} \quad (22)$$

with β_0 and β_1 as the first two coefficients of the QCD β -function

$$\begin{aligned} \beta_0 &= \frac{1}{3} (11C_A - 2n_f) \\ \beta_1 &= \frac{1}{3} (34C_A^2 - 2n_f(5C_A + 3C_F)), \end{aligned} \quad (23)$$

where $C_F = \frac{N_c^2 - 1}{2N_c}$ and $C_A = N_c$ are the Casimir operators in the fundamental and adjoint representations of the $SU(N_c)$ color group with $N_c = 3$. Λ is the QCD cut-off parameter and has been extracted from ZEUS data with $\alpha_s(M_Z^2) = 0.1166$. The following results have been obtained for Λ with four active flavor numbers (i.e., $n_f = 4$) as [29]

$$\Lambda^{\text{LO}} = 136.8 \text{ MeV}, \quad \Lambda^{\text{NLO}} = 284.0 \text{ MeV}. \quad (24)$$

The longitudinal structure function $F_L(x, Q^2)$ with the explicit form of the gluon density at the LO and NLO approximations is extracted due to the expansion points $0 \leq \alpha < 1$. To present more detailed discussions on our findings, the results for the longitudinal structure function are compared with the CT18 [30] parametrization model in the general mass-variable flavor number scheme (GM-VFNS) and in the zero mass-variable flavor number scheme (ZM-VFNS).

The GM-VFNS is dependent on the rescaling variable χ^1 where $\chi = x \left(1 + \frac{4m_c^2}{Q^2} \right)$, as the rescaling variable reduces to

¹ In order to account for the production threshold effect for the charm quark at $n_f = 4$, one should consider the quark mass for small Q^2 .

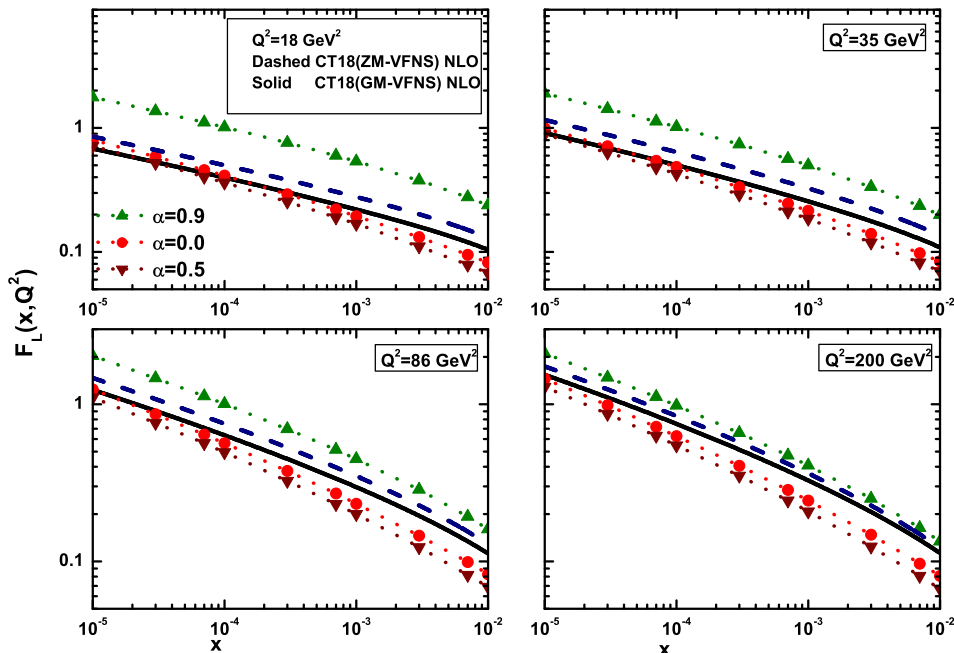


FIG. 1: The longitudinal structure function $F_L(x, Q^2)$ plotted at fixed Q^2 as a function of x variable for $\alpha = 0.0$ (red circles), $\alpha = 0.5$ (brown down-triangles) and $\alpha = 0.9$ (green up-triangles), compared with the CT18 parametrization method [30] in the GM-VFNS (solid curves) and in the ZM-VFNS (dashed curves) at the NLO approximation.

the Bjorken variable x at high Q^2 values. The data are taken from the H1-Collaboration [15] at HERA in the region $1.5 \leq Q^2 \leq 800 \text{ GeV}^2$ with a lepton beam energy of 27.6 GeV and two proton beam energies of $E_p = 460$ and 575 GeV corresponding to center-of-mass (COM) energies of 225 and 252 GeV, respectively from the inclusive ep double differential cross sections for neutral current deep inelastic scattering.

We have calculated the x -dependence of the longitudinal structure function at several fixed values of Q^2 corresponding to H1-Collaboration data in a wide range of the expansion point $z = \alpha$. Results are presented in Figure 1 where the x -evolution of $F_L(x, Q^2)$ is clearly exhibited for $\alpha = 0.0$ (red circles), $\alpha = 0.5$ (brown down-triangles) and $\alpha = 0.9$ (green up-triangles). It is seen that, for low values of the presented Q^2 , the extracted longitudinal structure function within the NLO approximation is in much better agreement with the CT18 parametrization model at $\alpha < 0.5$. Also, for high values of the presented Q^2 , the extracted longitudinal structure function within the NLO approximation is in a much better agreement with the CT18 parametrization model at $\alpha > 0.5$. We have found that the choice of $\alpha \sim 0.0$ and $\alpha \sim 0.9$ for the expansion points at low and high Q^2 values gives results that are sufficiently accurate for our purposes respectively.

In Fig.2, we present the x dependence of the longitudinal structure function at $Q^2 = 8.5$ and 200 GeV^2 compared with the H1 Collaboration data [15] accompanied by total errors and the results from CT18 (GM-VFNS) NLO parametrization model. We observe that, with respect to the expansion points used in the gluon density, the extracted longitudinal structure functions within the NLO approximation are comparable with the experimental data and the CT18 NLO model.

In Fig. 3, we show the Q^2 dependence of the longitudinal structure function at small x at the NLO approximation at fixed values of the invariant mass W as $W = 230 \text{ GeV}$. In this figure (i.e., Fig. 3), the results of calculations at the expansion points $\alpha = 0.0$ and 0.9 and the comparison with the H1 Collaboration data [15] accompanied by total errors are presented. The extracted values in a wide range of the expansion points are in good agreement with experimental data at low and high Q^2 values.

In conclusion, we have presented a method based on the expansion of gluon density to determine the longitudinal

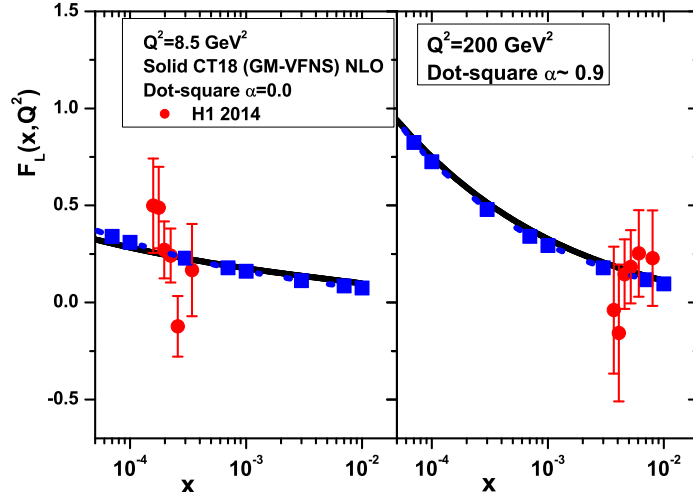


FIG. 2: The longitudinal structure functions at the NLO approximation with respect to the expansion points extracted in comparison with the H1 experimental data (red circles) [15] accompanied with total errors and the CT18 NLO [30] parametrization model.

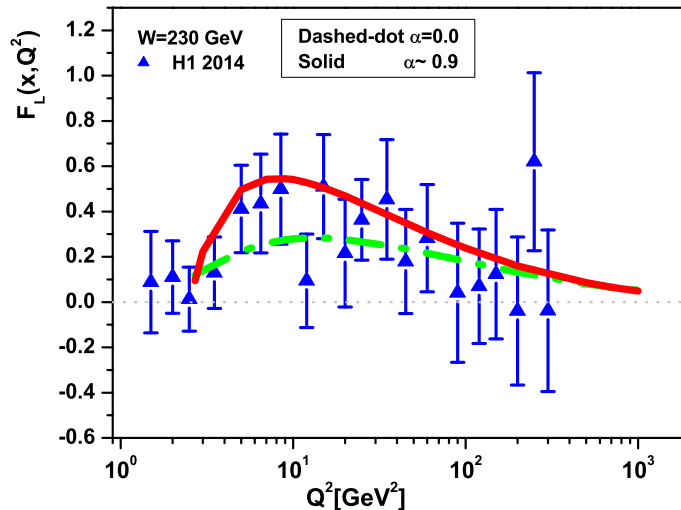


FIG. 3: The extracted longitudinal structure functions $F_L(x, Q^2)$ at a fixed value of the invariant mass W as $W = 230$ GeV at the expansion points $\alpha = 0.0$ (dashed-dot curve) and 0.9 (solid curve) compared with the H1 Collaboration data [15] accompanied with total errors.

structure function at the NLO approximation at low x . This method relies on the momentum carried by the gluon density due to the expansion points within a kinematical region characterized by low values of the Bjorken variable x . We find that the expansion method of gluon density provides correct behaviors of the extracted longitudinal structure function $F_L(x, Q^2)$ at low and high Q^2 values due to the expansion points $\alpha \simeq 0.0$ and 0.9 and that our results for $F_L(x, Q^2)$ demonstrate comparability with data from the H1 Collaboration, the CT18 parametrization method and other results obtained using the momentum space method [31].

ACKNOWLEDGMENTS

G.R.Boroun is grateful to Razi University for the financial support of this project.

-
- [1] W. J. Marciano, and H. Pagels, Phys. Rept. **36**, 137 (1978).
 - [2] J. D. Bjorken, and A. Paschos Emmanuel, Phys. Rev. **185**, 1975 (1969).
 - [3] E. Perez, and E. Rizvi, Rept. Prog. Phys. **76**, 046201 (2013).
 - [4] M. Breidenbach, J. I. Friedman, et al., Phys. Rev. Lett. **23**, 935 (1969).
 - [5] E. D. Bloom, D. H. Coward, et al., Phys. Rev. Lett., **23**, 930 (1969).
 - [6] H1 and ZEUS Collaborations, Eur. Phys. J. C **75**, 580 (2015).
 - [7] R. Abdul Khalek et al., Nucl. Phys. A **1026**, 122447 (2022).
 - [8] D. P. Anderle et al., Front. Phys. (Beijing) **16**, 64701 (2021).
 - [9] C. G. Callan, D. J. Gross, Phys. Rev. Lett. **22**, 156 (1969).
 - [10] C. Adloff et al. [H1 Collaboration], Phys. Lett. B **393**, 452 (1997).
 - [11] F.D. Aaron et al. [H1 Collaboration], Phys. Lett. B **665**, 139 (2008).
 - [12] F.D. Aaron et al. [H1 Collaboration], Eur. Phys. J. C **71**, 1579 (2011).
 - [13] S. Chekanov et al. [ZEUS Collaboration], Phys. Lett. B **682**, 8 (2009).
 - [14] F.D. Aaron et al. [H1 Collaboration], JHEP **09**, 061 (2012).
 - [15] V. Andreev et al. [H1 Collab.], Eur. Phys. J. C **74**, 2814 (2014).
 - [16] G. Altarelli and G. Martinelli, Phys. Lett. B **76**, 89 (1978).
 - [17] A. M. Cooper-Sarkar et al., Z. Phys. C **39**, 281 (1988).
 - [18] G. R. Boroun and B. Rezaei, Eur. Phys. J. C **72**, 2221 (2012).
 - [19] J. X. Chen, X. P. wang et al., Chin. Phys. C **48**, 063104 (2024).
 - [20] K.Prytz, Phys.Lett.B **311**, 286 (1993); Phys.Lett.B **332**, 393 (1994).
 - [21] K. Bora and D. K. Choudhury, Phys. Lett. B **354**, 151 (1995).
 - [22] M. B. Gay Ducati and P. B. Goncalves, Phys. Lett. B **390**, 401 (1997).
 - [23] V. N. Gribov and L. N. Lipatov, Sov. J. Nucl. Phys. **15**, 438 (1972).
 - [24] G. Altarelli and G. Parisi, Nucl. Phys. B **126**, 298 (1977).
 - [25] Y. L. Dokshitzer, Sov. Phys. JETP **46**, 641 (1977).
 - [26] A. Buckley et al., Eur. Phys. J. C **75**, 132 (2015).
 - [27] A. Accardi et al., Phys. Rev. D **93**, 114017 (2016).
 - [28] S. Moch, J.A.M. Vermaseren, and A. Vogt, Phys. Lett. B **606**, 123 (2005).
 - [29] L. P. Kaptari, A. V. Kotikov, N. Yu. Chernikova, and P. Zhang, Phys. Rev. D **99**, 096019 (2019).
 - [30] T.-J. Hou et al., Phys. Rev. D **103**, 014013 (2021).
 - [31] G.R.Boroun and P.Ha, Phys.Rev.D **109**, 094037 (2024).